Date: September 23, 2008
Version: 1.0 Preliminary
Editors: Anna Kropivnitskaya (kropiv@mail.desy.de), Andrei Rostovtsev (rostov@itep.ru)
Referees: Eddi de Wolf (Eddi.DeWolf@ua.ac.be), Tim Greenshaw (green@liverpool.ac.uk)
Deadline for comments:

Inclusive Photoproduction of $\rho(770)^0$, $\mathrm{K}^*(892)^0$ and $\phi(1020)$ Mesons at HERA (version of September 23, 2008)

H1 Collaboration

Abstract

Inclusive non-diffractive photoproduction of $\rho(770)^0$, $K^*(892)^0$ and $\phi(1020)$ mesons is investigated with the H1 detector in ep collisions at HERA. The corresponding average γp centre-of-mass energy is 210 GeV. The mesons are measured in the transverse momentum range $0.5 < p_T < 7$ GeV and rapidity range $|y| < 1$. The differential cross-sections are presented as a function of transverse momentum and rapidity and are compared to the predictions of Monte Carlo models and to data from other experiments.

To be submitted to *Eur. Phys. J.* **C**

1 Introduction

High energy particle collisions which give rise to large multiplicities of produced hadrons provide an opportunity to study the hadronisation process, whereby quarks and gluons convert to colourless hadrons. Since most hadrons are produced at low values of transverse momentum, the theory of perturbative quantum chromodynamics (pQCD) is not applicable to describe hadronisation. The most successful phenomenological models to describe the hadronisation process are the string [1] and the cluster fragmentation [2] models. However, these models depend on numerous parameters and need to be tuned to data.

The production of long-lived hadrons and resonances was studied in detail in electron-positron (e^+e^-) collisions at LEP using Z^0 decays [3]. The measurements in high energy hadronic interactions were restricted to long-lived and heavy quark hadrons. Recently, the production of the hadronic resonances $\rho(770)^0$, $K^*(892)^0$ and $\phi(1020)$ [4] has been measured in heavy-ion and proton-proton (pp) collisions at RHIC. The electron-proton (ep) collider HERA allows the study of particle production in quasi-real photon-proton (γp) collisions, where the nuclear density is much lower than that at RHIC. This study is particularly interesting, since the γp collision energy at HERA is about the same as the centre-of-mass energy of the colliding nucleons at RHIC.

In this paper, measurements of the inclusive non-diffractive photoproduction of the resonances $\rho(770)^0$, $K^*(892)^0$ and $\phi(1020)$ at HERA are presented for the first time. The measurements are based on the data recorded with the H1 detector during the year 2000, when positrons of energy 27.6 GeV collided with 920 GeV protons at an ep centre-of-mass energy of 319 GeV providing on average a γp centre-of-mass energy $<W>$=210 GeV. The data correspond to an integrated luminosity of $\mathcal{L} = 36.5$ pb^{-1}.

2 Phenomenology and Monte Carlo Simulation

The invariant differential cross-section for meson production can be expressed as a function of the meson's transverse momentum p_T and its rapidity y only, assuming azimuthal symmetry. The laboratory frame rapidity y (also y_{lab}) of a particle with energy E and longitudinal momentum p_z is given by $y = 0.5\ln\{(E + p_z)/(E - p_z)\}$. In hadronic collisions for central rapidities the produced hadrons are approximately uniformly distributed in rapidity, while the transverse momentum spectra fall steeply with increasing p_T. It is convenient to approximate the invariant differential cross-section of the produced hadrons with a damped power law distribution,

$$\frac{1}{\pi}\frac{d^2\sigma^{\gamma p}}{dp_T^2 dy} = \frac{A}{(E_{T_0} + E_T^{kin})^n} , \qquad (1)$$

where $E_T^{kin} = \sqrt{m_0^2 + p_T^2} - m_0$ is the transverse kinetic energy, m_0 is the nominal resonance mass and A is a normalisation factor. At low E_T^{kin} the damped power law function (1) is reduced to a Boltzmann-like exponential distribution proportional to $\exp(-E_T^{kin}/T)$, with $T = E_{T_0}/n$. This exponential behaviour of hadronic spectra was interpreted within a thermodynamic picture of hadroproduction [5]. In this framework the parameter T plays the role of the temperature at which hadronisation takes place. At high E_T^{kin} the function (1) is reduced to a power law distribution ($E_{T_0} = 0$) as expected from pQCD. The exponent n is defined in pQCD by a convolution of the parton densities of the colliding particles and the differential cross-sections of parton-parton interactions. The normalisation coefficient A is defined by the following condition:

$$\frac{d\sigma}{dy} = \int_0^\infty \frac{d^2\sigma^{\gamma p}}{dp_T^2 dy} dp_T^2 = \int_0^\infty \frac{A\pi}{(E_{T_0} + E_T^{kin})^n} dp_T^2 ,$$

which results in

$$A = \frac{d\sigma}{dy} \frac{(n-1)(n-2)(E_{T_0})^{n-1}}{2\pi(E_{T_0} + (n-2)m_0)} ,$$

where $d\sigma/dy$ is the differential photoproduction cross-section integrated over the full range in p_T.

Monte Carlo calculations are used for a comparison with the data. Direct and resolved photoproduction events are simulated using both the PYTHIA 6.2 [6] and the PHOJET 10 [7] Monte Carlo generators. The simulation of hadronisation is based for both generators on the string fragmentation model [8]. For data corrections the parameter setting tuned by the ALEPH collaboration [9] is used for the fragmentation of partons. The effect of Bose-Einstein correlations (BEC) on the invariant mass spectra of like-sign and unlike-sign pion pairs is included by using a Gaussian parametrisation for the Bose-Einstein enhancement [9]. The photoproduction events generated using PYTHIA and PHOJET are passed through a simulation of the H1 detector based on GEANT [10] and through the same reconstruction and analysis chain as used for the data. The simulated event samples are used to correct the data for detector effects.

3 Experimental Conditions

3.1 H1 Detector

The H1 detector is described in detail elsewhere [11]. A brief account of the components that are most relevant to the present analysis is given here. The H1 coordinate system convention defines the outgoing proton beam direction as the positive z-axis, also referred to as the “forward” direction. The polar angle θ is defined with respect to this direction. The pseudorapidity is given by $\eta = -\ln(\tan(\theta/2))$.

The central ep interaction region is surrounded by two large concentric drift chambers (CJCs), operated inside a 1.16 T solenoidal magnetic field. Charged particles are measured in the pseudorapidity range $-1.5 < \eta < 1.5$ with a transverse momentum resolution of $\sigma_{p_T}/p_T \approx 0.009 \cdot p_T[\text{GeV}] \oplus 0.015$. The specific energy loss dE/dx of the charged particles is measured in this detector with a resolution $\sigma(dE/dx)/(dE/dx)$ of 7.5% for a minimum ionising track.

A finely segmented electromagnetic and hadronic liquid argon calorimeter (LAr) covers the range $-1.5 < \eta < 3.4$. The energy resolution is $\sigma(E)/E = 0.11/\sqrt{E/\mathrm{GeV}}$ for electromagnetic showers and $\sigma(E)/E = 0.50/\sqrt{E/\mathrm{GeV}}$ for hadrons as measured in the test beam [12].

Photoproduction events are selected with a crystal Čerenkov calorimeter located close to the beam pipe at $z = -33.4$ m in the positron beam direction (positron tagger), which measures the energy deposited by positrons scattered at angles of less than 5 mrad. Another Čerenkov calorimeter, located at $z = -103$ m (photon tagger), is used to determine the ep luminosity by detecting the radiated photon emitted in the Bethe-Heitler process $ep \to e'p'\gamma$.

3.2 Event Selection

Photoproduction events are selected by a trigger which requires a scattered positron to be measured in the positron tagger, a reconstructed event vertex and three charged tracks reconstructed in the CJCs with transverse momentum $p_T > 0.4$ GeV for each of them. For these events, the photon virtuality Q^2 is smaller than 0.01 GeV^2. The energy measured by the positron tagger is used in the determination of the total γp collision energy W.

In order to reduce the non-ep background and to ensure good reconstruction of the event kinematics, the following selection criteria are applied for this analysis:

- Events are selected, if the reconstructed γp centre-of-mass energy lies within the interval $174 < W < 256$ GeV for which good positron efficiency is established. This corresponds to an average γp centre-of-mass energy of $<W>= 210$ GeV.
- In order to suppress random coincidences of the Bethe-Heitler events, which have a high rate, and beam-gas background in the main H1 detector, events are rejected, if a photon with energy $E_\gamma > 2$ GeV is detected in the photon tagger.
- The event vertex reconstructed from the tracks of charged particles is required to lie within ± 35 cm of the nominal z–position of the interaction point as defined by the longitudinal size of the proton bunch.

The trigger requirement suppresses elastic and diffractive events. Diffractive reactions are defined by $X_{I\!P} < 0.05$, with $X_{I\!P} = M_X^2/W^2$, where M_X is the invariant mass of the hadronic diffractive system. To further suppress the contribution of diffractive processes in the selected sample, the presence of an energy deposition of at least 500 MeV is required in the forward region of the LAr, defined by $2.03 < \eta < 3.26$. After applying this requirement, the final event sample contains less than 1% of diffractive events.

In total, about 1.8×10^6 events satisfy the above selection criteria.

3.3 Selection of $\rho(770)^0$, K$^*(892)^0$ and $\phi(1020)$ Mesons

The mesons are identified using the $\rho(770)^0 \to \pi^+\pi^-$, $K^*(892)^0 \to K^+\pi^-$ or $\overline{K}^*(892)^0 \to K^-\pi^+$ and $\phi(1020) \to K^+K^-$ decays[1]. Charged tracks reconstructed in the CJCs with $p_T > 0.15$ GeV and pseudorapidity $|\eta| < 1.5$ are considered as charged pion or kaon candidates. Since most charged particles in ep collisions are pions, no attempt to separate pions from kaons is made, while identification criteria for the charged kaons are applied for the extraction of the K^{*0} and $\phi(1020)$ signals. This is done by measuring the momentum dependent specific energy loss dE/dx in the CJCs. This method gives a significant improvement in the signal to background ratio for mesons at low p_T ($p_T < 1.5$ GeV), where the dE/dx resolution allows good particle identification. For mesons at high p_T ($p_T > 1.5$ GeV), the dE/dx method is inefficient and particle identification is not used. The rapidity range for the reconstructed neutral mesons is restricted to $|y| < 1$.

To extract the ρ^0, K^{*0} and $\phi(1020)$ signals, the respective invariant mass distributions of their decay products, $m(\pi^+\pi^-)$, $m(K^\pm\pi^\mp)$ and $m(K^+K^-)$, are fitted using a function composed of three parts,

$$F(m) = B(m) + \sum R(m) + \sum S(m). \tag{2}$$

The terms correspond to the contributions due to the combinatorial background $B(m)$, to reflections $R(m)$ and to the sum of the relevant signals $S(m)$, respectively.

The combinatorial background function $B(m)$ for the ρ^0 and K^{*0} is taken to be the invariant mass distribution of like-sign combinations $m(\pi^\pm\pi^\pm)$ from data for ρ^0 or $m(K^\pm\pi^\pm)$ for K^{*0}, multiplied by a third order polynomial. The shape of the combinatorial background for $\phi(1020)$ is described by the following function:

$$B(m) = a_1(m^2 - 4m_K^2)^{a_2} e^{-a_3 m}\,,$$

where a_1, a_2 and a_3 are free parameters and m_K is the kaon mass.

The second term $\sum R(m)$ in (2) represents the sum of the reflections; for example charged particles from decay of the $K^{*0} \to K^\pm\pi^\mp$ with the kaon misidentified as a charged pion will give a structure in the $m(\pi^+\pi^-)$ spectrum and must be taken into account as a separate contribution. In addition, there are two other contributions to the $m(\pi^+\pi^-)$ spectrum in the mass region of interest: from the decays $\omega(782) \to \pi^+\pi^-$ and $\omega(782) \to \pi^+\pi^-\pi^0$ in which the π^0 is not observed. The five major reflections in the $m(K^\pm\pi^\mp)$ spectrum are due to: the decay $\rho^0 \to \pi^+\pi^-$ with the π^+ or π^- misidentified as a charged kaon, the decays $\omega(782) \to \pi^+\pi^-$ and $\omega(782) \to \pi^+\pi^-\pi^0$ with the π^0 not observed and with one of the π^+ or π^- mesons misidentified as a charged kaon, the decay $\phi(1020) \to K^+K^-$ with one of the kaons misidentified as a charged pion and a self-reflection from the K^{*0}, where the pion and kaon are mistakenly interchanged. For the $m(K^+K^-)$ spectrum there are no reflections in the invariant mass region of interest. The shape of the reflections are taken from the Monte Carlo calculations. The

[1] In the following, the notation K^{*0} is used to refer to both the K^{*0} and $\overline{K}^{*0}$ mesons unless explicitly stated otherwise.

amount of reflections from ρ^0, K^{*0} and $\phi(1020)$ mesons corresponds to the production rates determined in this analysis. For $\omega(782)$ the production rate relative to that of ρ^0 is varied within the range 1.0 ± 0.2, which is consistent with measurements of the $\omega(782)/\rho^0$ ratio in hadronic collisions [13] and in Z^0 boson decays [14].

The function $S(m)$ used to describe the signal in (2) is a convolution of a relativistic Breit-Wigner function $BW(m)$ and a resolution function $r(m, m')$, which accounts for the uncertainty in the momentum measurement using CJCs. The Breit-Wigner function

$$BW(m) = A_0 \, \frac{m_0 m \Gamma(m)}{(m^2 - m_0^2)^2 + m_0^2 \Gamma^2(m)} \; , \tag{3}$$

is used with

$$\Gamma(m) = \Gamma_0 \left(\frac{q}{q_0}\right)^{2l+1} \frac{m_0}{m} \; ,$$

where A_0 is a normalisation factor, Γ_0 is the resonance width, $l = 1$ for vector mesons, m_0 is the resonance mass, q is the momentum of the decay products in the rest frame of the parent, and q_0 is their momentum at $m = m_0$. Monte Carlo studies have revealed that a non-relativistic Breit-Wigner, with width Γ_{res}, is a good representation for $r(m, m')$:

$$r(m, m') = \frac{1}{2\pi} \, \frac{\Gamma_{res}}{(m - m')^2 + (\Gamma_{res}/2)^2} \; . \tag{4}$$

For the K^{*0} analysis the resolution parameter Γ_{res} is determined from Monte Carlo and is equal to about 12 MeV. The mass resolution is about four times smaller than the width of the K^{*0} meson (50.3 ± 0.6 MeV) [15], leading only to a small change in the shape of the resonance. For the $\phi(1020)$ the mass resolution is comparable to the width of the ϕ meson ($\Gamma_0 = 4.25 \pm 0.05$ MeV) [15]. As a result, the shape of the ϕ signal is significantly changed, and the resolution Γ_{res} is taken as a free parameter in the fit and varies from 3.4 MeV to 6.0 MeV, increasing with the p_T of the ϕ meson.

For the ρ^0 the mass reconstruction resolution is significantly smaller than the natural width. However, BEC strongly distort the ρ^0 shape through interactions between the ρ^0 decay pions and other pions. The BEC plays an important role in broadening the ρ^0 mass peak and in shifting it towards lower masses. A similar effect was observed in pp and heavy-ion collisions at RHIC [4] and in e^+e^- collision at LEP using Z^0 decays [14]. It is therefore important to check that the Monte Carlo model used for the extraction of the cross-section describes the di-pion spectra in the data. The data spectra and the Monte Carlo simulations with and without BEC effects are shown in figure 1. The Monte Carlo model with BEC is found to be in a good agreement with the data, whereas the model without BEC fails to describe the di-pion mass spectrum in the region of the ρ^0 resonance.

For p_T of the ρ^0 meson less than 0.5 GeV the effect of BEC on the ρ^0 shape becomes strong and Monte Carlo is not able to describe the data. Moreover, in the p_T region less than 0.5 GeV of the mesons, it is not possible to reliably extract K^{*0} or $\phi(1020)$ signals due to the high background and low efficiency of reconstruction. For these reasons, this analysis is restricted to p_T of the hadronic resonances larger than 0.5 GeV.

The results of fitting the function (2) to the $m(\pi^+\pi^-)$ data in the mass range from 0.55 to 1.7 GeV with the contributions due to the combinatorial background and the reflections are shown in figures 2a and 2b. In this mass range the signal from $f_0(980)$ and $f_2(1270)$ was taken into account and fitted with the relativistic Breit-Wigner function given in equation (3). In the fit, the nominal resonance masses m_0 were left free, while the ρ^0, $f_0(980)$ and $f_2(1270)$ widths were fixed to the Particle Data Group [15] values. Due to the small signal and non-trivial background behaviour, it is not possible to measure the production cross-section for the $f_0(980)$ and $f_2(1270)$ mesons.

The K^{*0} signal is measured under the assumption that there is no difference between the particle and antiparticle production rates, and the signal obtained from the $m(K^\pm\pi^\mp)$ spectrum is divided by 2 to get the K^{*0} rate. The result of fitting the function (2) to the $m(K^\pm\pi^\mp)$ data in the mass range from 0.7 to 1.2 GeV with the contributions due to the combinatorial background and the reflections is shown in figure 2c. In the fit, the K^{*0} width is fixed to the Particle Data Group value [15] while the mass parameter is left free. The result for the K^{*0} mass is compatible with [15].

The result of fitting the function (2) to the $m(K^+K^-)$ data in the mass range from 0.99 to 1.06 GeV together with the background contribution is shown in figure 2d. In the fit the ϕ width Γ_0 is fixed to the Particle Data Group value [15] while the mass is a free parameter. The results for the ϕ mass are compatible with [15].

3.4 Cross-section Determination and Systematic Errors

The invariant differential cross-section of ρ^0, K^{*0} and $\phi(1020)$ meson production is calculated according to

$$\frac{1}{\pi}\frac{d^2\sigma^{\gamma p}}{dp_T^2 dy} = \frac{N(p_T, y)}{\pi \cdot \mathcal{L} \cdot \epsilon \cdot BR \cdot \Phi_\gamma \cdot \Delta p_T^2 \cdot \Delta y},$$

where $N(p_T, y)$ is the number of mesons from the fit in a bin of y and p_T. The corresponding bin widths are Δy and $\Delta p_T^2 = 2p_T^{bin}\Delta p_T$. Bin centre corrections are applied to define the value of p_T^{bin} at which the differential cross-section is measured. The number of observed mesons is defined by the integral over the signal function determined from the invariant mass fit for each meson within $\pm 2.5\Gamma_0$ of its nominal mass. $\mathcal{L}$ denotes the integrated luminosity. The product of the reconstruction and trigger efficiency and the positron tagger acceptance is given by ϵ. The reconstruction efficiency for the mesons is above 45% at low p_T and rises to about 90% with p_T increasing. The trigger efficiency is extracted from Monte Carlo and data using monitor triggers and is found to vary between 40% and 80%. The average acceptance of the positron tagger is about 50% which is determined as in [16]. The branching fractions BR used in the correction procedure are taken from [15] and are equal to 1, 0.67 and 0.49 for $\rho^0 \to \pi^+\pi^-$, $K^{*0} \to K^\pm\pi^\mp$ and $\phi(1020) \to K^+K^-$, respectively. The photon flux $\Phi_\gamma = 0.0127$ is calculated assuming the Weizsäcker-Williams approximation [17]. The data sample is divided into four bins in rapidity from -1 to 1 and seven bins in transverse momentum from 0.5 to 7 GeV.

The statistical error varies from $7-15\%$ for the ρ^0, $10-18\%$ for the K^{*0} and $13-24\%$ for the $\phi(1020)$ mesons. The systematic error consists of the uncertainties of the track reconstruction efficiency (3%), the trigger efficiency (up to 6%), the variation of the $f_0(980)$ width from 40 to 100 MeV for the ρ^0 fit (up to 7% in the low p_T bins), of the uncertainties in the dE/dx kaon identification procedure (6% for the K^{*0} and 8% for the $\phi(1020)$), the luminosity calculation (2%), background shape variation (5%) and the variation of the assumptions about the normalisation of the contributions from the reflections (4% for the ρ^0 and up to 15% for the K^{*0}). The total systematic error is in the range $10-12\%$ for the ρ^0, $10-18\%$ for the K^{*0} and $9-17\%$ for the $\phi(1020)$ meson cross-sections.

4 Results and Discussion

The inclusive non-diffractive photoproduction cross-sections for ρ^0, K^{*0} and $\phi(1020)$ mesons in the kinematic region $Q^2 < 0.01$ GeV^2, $174 < W < 256$ GeV and in the visible phase space of the mesons $p_T > 0.5$ GeV and $|y| < 1$ is found to be

$$\sigma^{\gamma p}_{vis}(\gamma p \to \rho^0 X) = 25600 \pm 1800 \pm 2600 \text{ nb},$$
$$\sigma^{\gamma p}_{vis}(\gamma p \to K^{*0} X) = 6260 \pm 350 \pm 840 \text{ nb},$$
$$\sigma^{\gamma p}_{vis}(\gamma p \to \phi X) = 2400 \pm 180 \pm 290 \text{ nb}\,.$$

The first error is statistical and the second is systematic. Here and in the following K^{*0} denotes the sum of particle and antiparticle divided by 2.

The differential cross-sections for the photoproduction of ρ^0, K^{*0}, and ϕ mesons are presented in tables 1 and 2 and in figure 3. Within the rapidity range of this measurement, the resonance production rates are flat as a function of rapidity, within errors. This allows to describe the transverse momentum spectra of the ρ^0, K^{*0} and ϕ mesons by the function (1), where $d\sigma/dy$ is represented by an average value of $<d\sigma/dy>_{|y|<1}$ for central rapidities. The value of the exponent n is fixed to 6.7, as derived previously from precise measurements of charged particle spectra by the H1 collaboration [18] with $n = 6.7 \pm 0.3$. The damped power law distribution, with the same value of n, describes K^0_S mesons and Λ^0 baryons [19] and $D^{*\pm}$ mesons [20] measured at HERA which are shown in figure 5. A similar shape of the transverse momentum distribution, but with different values of the parameters n and E_{T_0}, was reported for charged particles produced in hadronic collisions [21]. The results of the fit of the measured differential cross-section for photoproduction of ρ^0, K^{*0} and ϕ mesons to the function (1) are shown in figure 3a. In table 3, the parameters of the fit and the average transverse kinetic energy $<E_T^{kin}>$ derived from (1), the average transverse energy $<E_T> = <E_T^{kin}> + m_0$ and the transverse momentum $<p_T> = \sqrt{<E_T>^2 - m_0^2}$ are presented. They are compared to those measured at RHIC in pp and gold-gold ($AuAu$) collisions and to PYTHIA predictions for photoproduction.

It is interesting to observe that the resonances with different masses, lifetimes and strangeness content are produced with about the same value of the average transverse kinetic energy $<E_T^{kin}>$. This observation supports the thermodynamic picture of hadronic interactions [5] , where the primary hadrons are thermalised during the interaction. The values of $< p_T >$ of ρ^0, K^{*0} and ϕ mesons are very similar in γp and pp collisions for about the same energy $\sqrt{s} \approx 200$ GeV, while they are all higher in $AuAu$ collisions. The PYTHIA simulations yield for the exponent $n = 6.85 \pm 0.06$ which is consistent with H1 data within errors. At the same time, as can be seen in table 3, the Monte Carlo model underestimates the values of the parameter $T = E_{T_0}/n$.

The measurements in the visible kinematic range of the ρ^0, K^{*0} and ϕ mesons, $p_T > 0.5$ GeV and $|y| < 1$, are extrapolated to the full p_T range in order to extract the total inclusive non-diffractive photoproduction cross-sections using fit the data to function (1). The extrapolation factors are found to be about 2. To calculate cross-section ratios the average values of the differential cross-sections $<d\sigma/dy>_{|y|<1}$ for the ρ^0, K^{*0} and ϕ mesons are used. In the rapidity interval $|y| < 1$ and integrated over the full p_T range the following ratios R are obtained:

$$R(K^{*0}/\rho^0) = 0.221 \pm 0.033 \ ,$$
$$R(\phi/\rho^0) = 0.078 \pm 0.012 \ ,$$
$$R(\phi/K^{*0}) = 0.354 \pm 0.055 \ .$$

The total error is given by the statistical and systematic error are added in quadrature. PYTHIA and PHOJET with the strangeness suppression factor $\lambda_s = 0.286$ [9] predict the following ratios 0.200, 0.055 and 0.277 respectively, which are lower than the measured ones. A value of the parameter $\lambda_s = 0.32^{+0.04}_{-0.07}$ is needed in these models to describe the data.

In figure 4 $R(\phi/K^{*0})$ is compared to the corresponding ratios measured by STAR in pp and $AuAu$ collision [4] at $\sqrt{s_{NN}} = 200$ GeV. The H1 result is in good agreement with the STAR pp ratio at a similar energy scale. The higher value for $R(\phi/K^{*0})$ measured in $AuAu$ collisions indicates an enhanced production of the $s\bar{s}$-quarkonium state compared to pp and γp interactions.

5 Conclusions

First measurements of inclusive non-diffractive photoproduction of $\rho(770)^0$, $K^*(892)^0$ and $\phi(1020)$ mesons at HERA are presented. The differential cross-sections for production of these resonances as a function of transverse momentum are described by a damped power law distribution while the differential cross-sections as a function of rapidity are observed to be flat, within errors in the visible range. It is observed that these resonances with their different masses, lifetimes and strangeness content are produced with about the same value of the average transverse kinetic energy. This observation supports a thermodynamic picture of hadronic interactions.

A modification of the shape of ρ^0 resonance produced in γp collisions at HERA is described by taking into account BEC in Monte Carlo models. A similar effect is observed in pp and heavy-ion collisions at RHIC and in e^+e^- annihilation at LEP, using Z^0 decays.

The cross-sections ratios $R(K^{*0}/\rho^0)$, $R(\phi/\rho^0)$ and $R(\phi/K^{*0})$ are estimated, and $R(\phi/K^{*0})$ is compared to results obtained in pp and heavy-ion collisions by the STAR experiment at RHIC. The ratio $R(\phi/K^{*0})$ measured in γp interactions is in agreement with pp results and is significantly below that for $AuAu$ interactions measured at about the same collision energy.

Acknowledgements

We are grateful to the HERA machine group whose outstanding efforts have made this experiment possible. We thank the engineers and technicians for their work in constructing and maintaining the H1 detector, our funding agencies for financial support, the DESY technical staff for continual assistance and the DESY directorate for support and for the hospitality which they extend to the non-DESY members of the collaboration.

References

[1] B. Andersson *et al.*, "Parton fragmentation and string dynamics," Phys. Rept. **97** (1983) 31.

[2] G.C. Fox and S. Wolfram, "A model for parton showers in QCD," Nucl. Phys. B **168** (1980) 285.

[3] A. Boehrer (Siegen U.), "Inclusive particle production in hadronic decays of the Z boson at LEP-1," Phys. Rept. **291** (1997) 107, and refereces herein.

[4] STAR Collab., J.Adams, *et al.*, "ρ^0 production and possible modification in $Au+Au$ and $p+p$ collisions at $\sqrt{s_{NN}}=200$ GeV," Phys. Rev. Lett. **92** (2004) 092301;
STAR Collab., C. Adler *et al.*, "$K(892)^*$ resonance production in $Au+Au$ and $p+p$ collisions at $\sqrt{s_{NN}}=200$ GeV at STAR," Phys. Rev. C **71** (2005) 064902;
STAR Collab., John Adams *et al.*, "ϕ meson production in $Au+Au$ and $p+p$ collisions at $\sqrt{s_{NN}}=200$ GeV," Phys. Lett. B **612** (2005) 181;
PHENIX Collab., S.S. Adler *et al.*, " Production of phi mesons at mid-rapidity in $\sqrt{s_{NN}}=200$ GeV $Au+Au$ collisions at RHIC" Phys. Rev. C **72** (2005) 014903.

[5] R. Hagedorn, "Statistical thermodynamics of strong interactions at high energies," Nuovo Cim. Suppl. **3** (1965) 147.

[6] T. Sjöstrand, Leif Lonnblad, Stephen Mrenna, LU-TP-01-21, "PYTHIA 6.2 physics and manual," hep-ph/0108264, (2001).

[7] R. Engel, "Photoproduction within the two component dual parton model. 1. Amplitudes and cross-sections," Z. Phys. C **66** (1995) 203;
R. Engel and J. Ranft, "Hadronic photon-photon interactions at high-energies," Phys. Rev. D **54** (1996) 4244.

[8] T. Sjöstrand, "High-energy physics event generation with PYTHIA 5.7 and JETSET 7.4," Comput. Phys. Commun. **82** (1994) 74.

[9] ALEPH Collab., S. Schael *et al.*, " Bose-Einstein correlations in W-pair decays with an event-mixing technique," Phys. Lett. B **606** (2005) 265; ALEPH Collab., G. Rudolph, private communication.

[10] R. Brun *et al.*, GEANT3 User's Guide, CERN-DD/EE/84-1.

[11] H1 Collab., I. Abt *et al.*, “The H1 detector at HERA,” Nucl. Instrum. Meth. A **386** (1997) 310 and 348.

[12] H1 Calorimeter Group, B. Andrieu *et al.*, “Results from pion calibration runs for the H1 liquid argon calorimeter and comparisons with simulations,” Nucl. Instrum. Meth. A **336** (1993) 499;
H1 Calorimeter Group, B. Andrieu *et al.*, “Beam tests and calibration of the H1 liquid argon calorimeter with electrons,” Nucl. Instrum. Meth. A **350** (1994) 57.

[13] Bonn-Hamburg-Munich Collab., V. Blobel *et al.*, “Observation of vector meson production in inclusive pp reactions,” Phys. Lett. B **48** (1974) 73.

[14] OPAL Collab., P.D. Acton *et al.*, “Inclusive neutral vector meson production in hadronic Z0 decays,” Z. Phys. C **56** (1992) 521;
ALEPH Collab., D. Busculic *et al.*, “Inclusive production of neutral vector mesons in hadronic Z decays,” Z. Phys. C **69** (1996) 379.

[15] W.-M. Yao *et al.*, “Review of particle physics,” J. Phys. G **33** (2006) 1.

[16] S. Aid *et al.*, “Measurement of the total photon-proton cross-section and its decomposition at 200 GeV center-of-mass energy,” Z. Phys. C **69** (1995) 27.

[17] C.F. Weizsäcker, “Radiation emitted in collisions of very fast electrons,” Z. Phys. **88** (1934) 612;
E.J. Williams, “Nature of the high-energy particles of penetrating radiation and status of ionization and radiation formulae,” Phys. Rev. **45** (1934) 729.

[18] H1 Collab., I. Abt *et al.*, “Inclusive charged particle cross-sections in photoproduction at HERA,” Phys. Lett. B **328** (1994) 176;
H1 Collab., C. Adloff *et al.*, “Charged particle cross-sections in photoproduction and extraction of the gluon density in the photon.” Eur. Phys. J. C **10** (1999) 363.

[19] H1 Collab., C. Adloff *et al.*, “Photoproduction of K^0 and Λ at HERA and a comparison with deep inelastic scattering,” Z. Phys. C **76** (1997) 213.

[20] H1 Collab., A. Aktas *et al.*, “Inclusive $D^{*\pm}$ meson cross-sections and $D^{*\pm}$-jet correlations in photoproduction at HERA,” Eur. Phys. J. C **50** (2007) 251.

[21] UA1 Collab., C. Albajar *et al.*, “A study of the general characteristics of proton - antiproton collisions at $\sqrt{s} = 0.2 - 0.9$ TeV,” Nucl. Phys. B **335** (1990) 261;
CDF Collab., F. Abe *et al.*, “Transverse momentum distributions of charged particles produced in anti-p p interactions at $\sqrt{s} = 630$ GeV and 1800 GeV,” Phys. Rev. Lett. **61** (1988) 1819.

$\frac{1}{\pi}\frac{d^2\sigma}{dydp_T^2}$ [nb/(GeV)^2]			
p_T [GeV] (p_T^{bin})	ρ^0	$(K^{*0}+\overline{K}^{*0})/2$	ϕ
$[0.5, 0.75](0.63)$	$5610 \pm 870 \pm 570$	$1190 \pm 130 \pm 190$	$383 \pm 54 \pm 50$
$[0.75, 1.0](0.87)$	$2440 \pm 180 \pm 250$	$621 \pm 68 \pm 78$	$264 \pm 34 \pm 31$
$[1.0, 1.5](1.22)$	$680 \pm 55 \pm 68$	$176 \pm 18 \pm 21$	$76 \pm 12 \pm 9$
$[1.5, 2.0](1.72)$	$142 \pm 15 \pm 14$	$48.0 \pm 5.2 \pm 4.9$	$19.1 \pm 3.3 \pm 1.8$
$[2.0, 3.0](2.41)$	$29.9 \pm 2.3 \pm 3.0$	$8.96 \pm 0.90 \pm 0.95$	$3.48 \pm 0.76 \pm 0.33$
$[3.0, 4.0](3.43)$	$3.06 \pm 0.42 \pm 0.32$	$1.21 \pm 0.17 \pm 0.13$	$0.46 \pm 0.11 \pm 0.08$
$[4.0, 7.0](5.09)$	$0.276 \pm 0.037 \pm 0.032$	$0.079 \pm 0.014 \pm 0.009$	$0.0335 \pm 0.0081 \pm 0.0056$

Table 1: Inclusive non-diffractive photoproduction invariant differential cross-sections $d^2\sigma/\pi dydp_T^2$ of $\rho(770)^0$, $K^*(892)^0$ and $\phi(1020)$ meson in the rapidity range $|y| < 1.0$ in bins of p_T. The first error is statistical and the second is systematic. For each bin in p_T the range as well as the bin-centre corrected (p_T^{bin}) value is given.

$d\sigma/dy$[nb]			
rapidity y	ρ^0	$(K^{*0}+\overline{K}^{*0})/2$	ϕ
$[-1.0, -0.5]$	$11000 \pm 1000 \pm 1100$	$3360 \pm 350 \pm 720$	$1440 \pm 250 \pm 180$
$[-0.5, 0.0]$	$13100 \pm 1100 \pm 1300$	$2520 \pm 270 \pm 350$	$1080 \pm 120 \pm 130$
$[0.0, 0.5]$	$10400 \pm 1500 \pm 1000$	$3070 \pm 300 \pm 430$	$1440 \pm 130 \pm 180$
$[0.5, 1.0]$	$14600 \pm 1300 \pm 1500$	$4280 \pm 440 \pm 780$	$1610 \pm 330 \pm 210$

Table 2: Inclusive non-diffractive photoproduction invariant differential cross-sections $d\sigma/dy$ of $\rho(770)^0$, $K^*(892)^0$ and $\phi(1020)$ meson in the transverse momentum $p_T > 0.5$ GeV in bins of y. The first error is statistical and the second is systematic.

	ρ^0	$(K^{*0}+\overline{K}^{*0})/2$	ϕ
$<d\sigma/dy>_{\vert y\vert<1}$ [nb]	23600 ± 2400	5220 ± 560	1850 ± 210
T [GeV]	0.151 ± 0.006	0.166 ± 0.008	0.170 ± 0.009
T^{PYTHIA} [GeV]	0.136	0.140	0.149
$<E_T>$ [GeV]	1.062 ± 0.014	1.205 ± 0.017	1.333 ± 0.020
$<E_T^{kin}>$ [GeV]	0.287 ± 0.014	0.313 ± 0.017	0.315 ± 0.020
$<p_T>$ [GeV]	0.726 ± 0.021	0.811 ± 0.025	0.860 ± 0.032
$<p_T>_{pp}$ [GeV]	0.616 ± 0.062	0.81 ± 0.14	0.82 ± 0.03
$<p_T>_{AuAu}$ [GeV]	0.83 ± 0.10	1.08 ± 0.14	0.97 ± 0.02

Table 3: The parameters $<d\sigma/dy>_{|y|<1}$ and $T = E_{T_0}/n$ for the ρ^0, K^{*0} and ϕ mesons from a fit of the function (1) to the differential cross-sections are presented. The average transverse energy $<E_T>$, kinetic energy $<E_T^{kin}>$ and momentum $<p_T>$ are shown and the latter are compared with results from pp and $AuAu$ collisions of the STAR experiment [4]. The temperature T is also compared to the value T^{PYTHIA} obtained from PYTHIA simulations. In H1 measurements, statistical and systematic error are summed in quadrature.

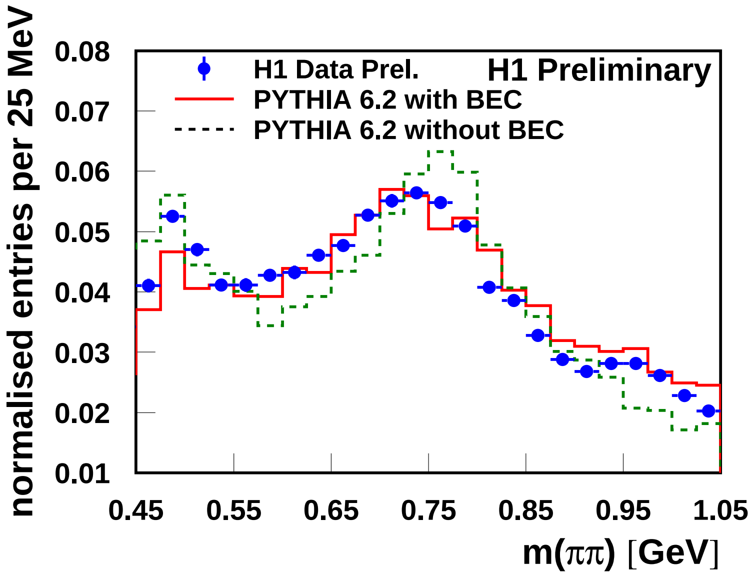

Figure 1: The unlike-sign mass spectrum with the like-sign spectrum subtracted. The full curve corresponds to the PYTHIA simulation with BEC and the dashed curve to the one without BEC.

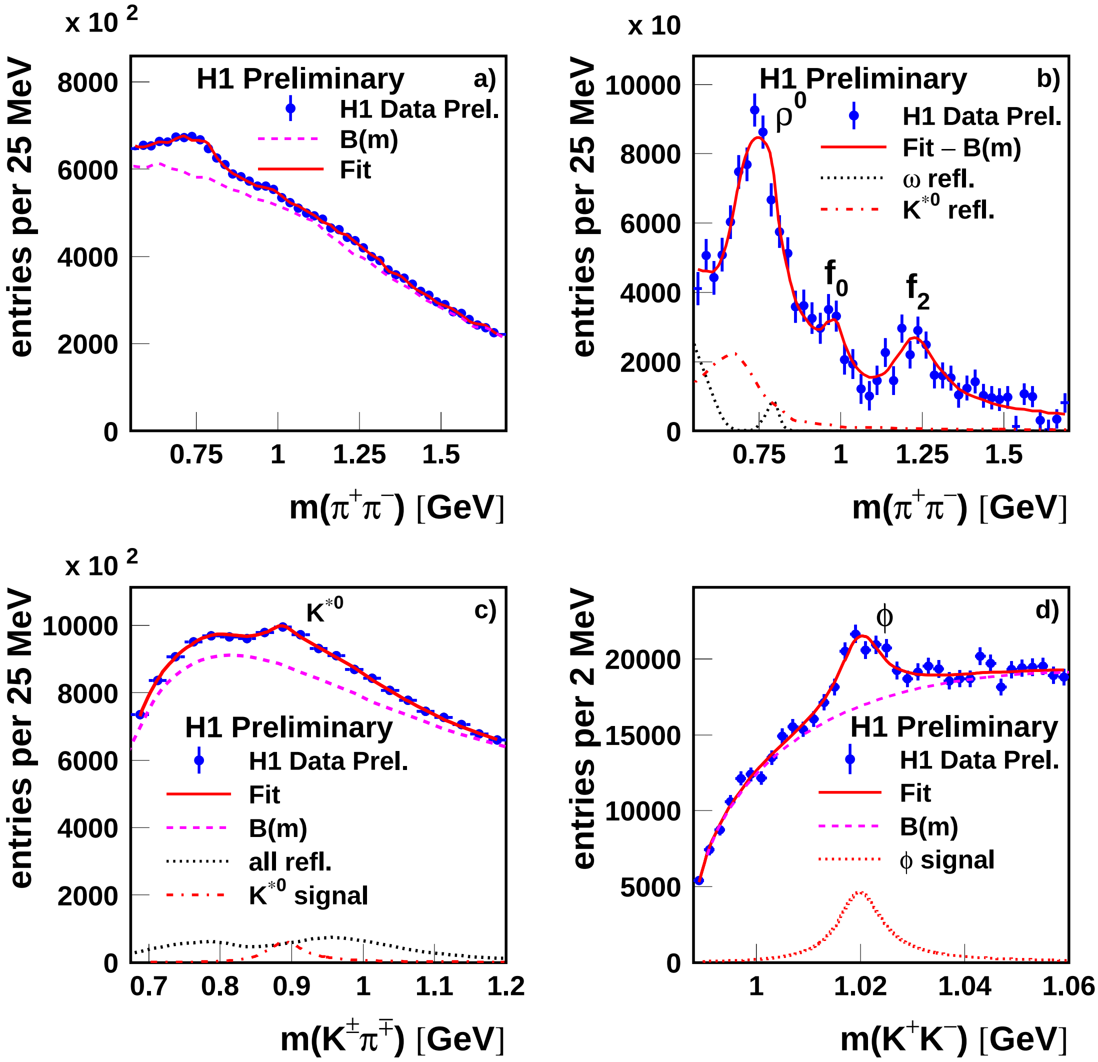

Figure 2: The invariant mass spectrum for $|y| < 1$ and $1.0 < p_T < 1.5$ GeV. For a): the full curve shows the result of the fit; the dashed curve corresponds to the contribution of the combinatorial background. For b): the full curve shows the result of the fit after subtraction of the combinatorial background $B(m)$; the dotted and dash-dotted curves describe the contributions from ω and K^* reflections, respectively. For c): the full curve shows the result of the fit; the dashed curve corresponds to the contribution of the combinatorial background; the dotted curve corresponds to the contribution of the reflections; the dash-dotted curve corresponds to the contribution of the K^* signal. For d): the full curve shows the result of the fit; the dashed curve corresponds to the contribution of the combinatorial background; the dotted curve corresponds to the contribution of the ϕ signal.

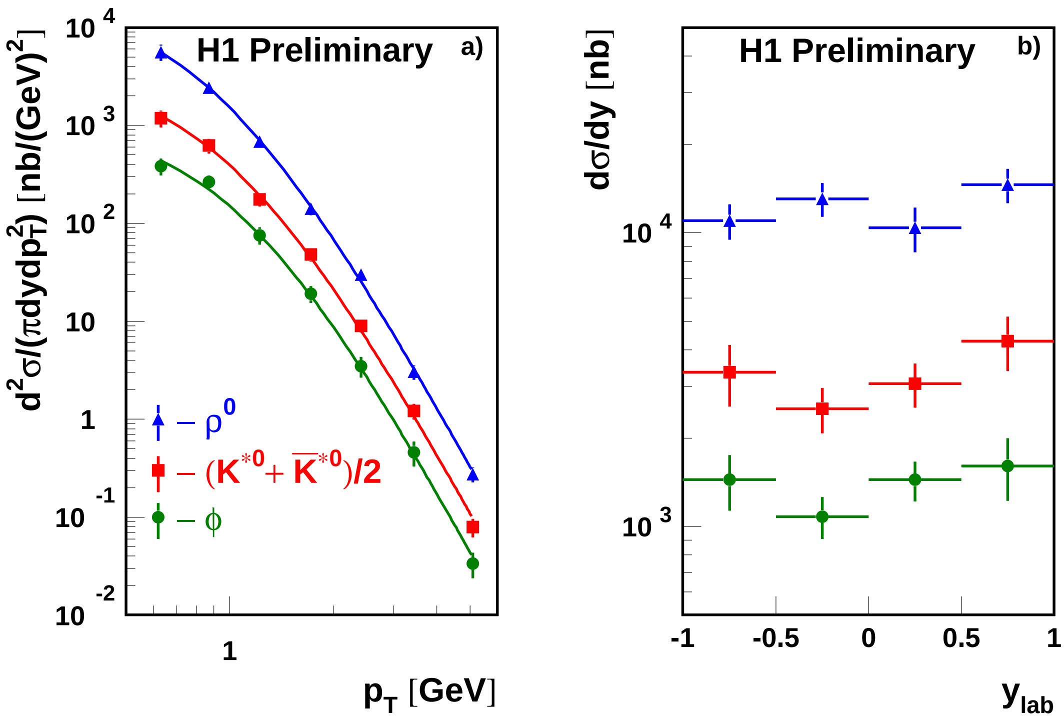

Figure 3: The differential non-diffractive cross-sections for ρ^0, K^{*0} and $\phi(1020)$ mesons plotted in $a)$ as a function of transverse momentum for $|y| < 1$ and in $b)$ as a function of rapidity for $p_T > 0.5$ GeV. The curves on the figure $a)$ correspond to a damped power law fit using equation (1). Statistical and systematic errors are added in quadrature on these plots.

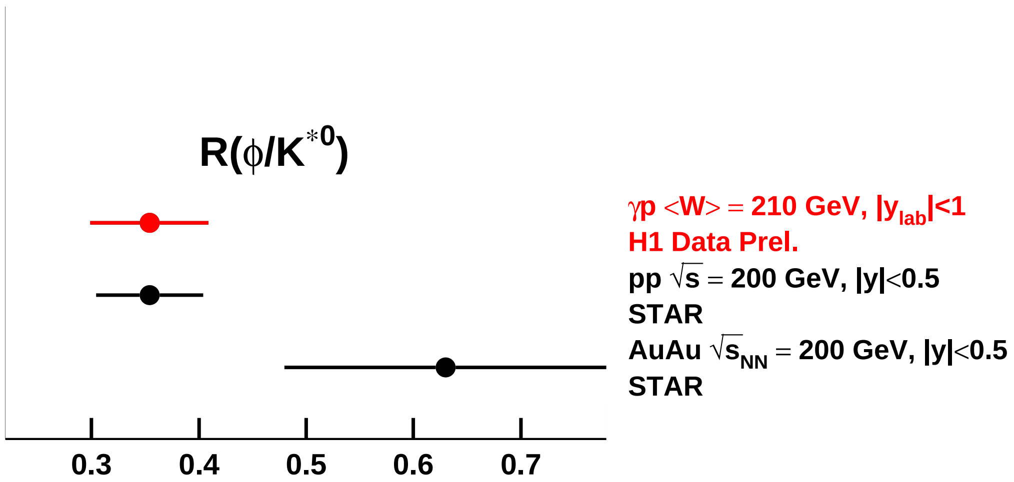

Figure 4: The ratio $R(\phi/K^{*0})$ of the total cross-sections. The ratio in γp collisions (H1) at $<W>= 210$ GeV is compared to measurements in $AuAu$ and in minimum bias pp interactions at $\sqrt{s_{NN}} = 200$ [4] at central rapidities. The errors at H1 correspond to the quadratic sum of the statistical and systematic errors.

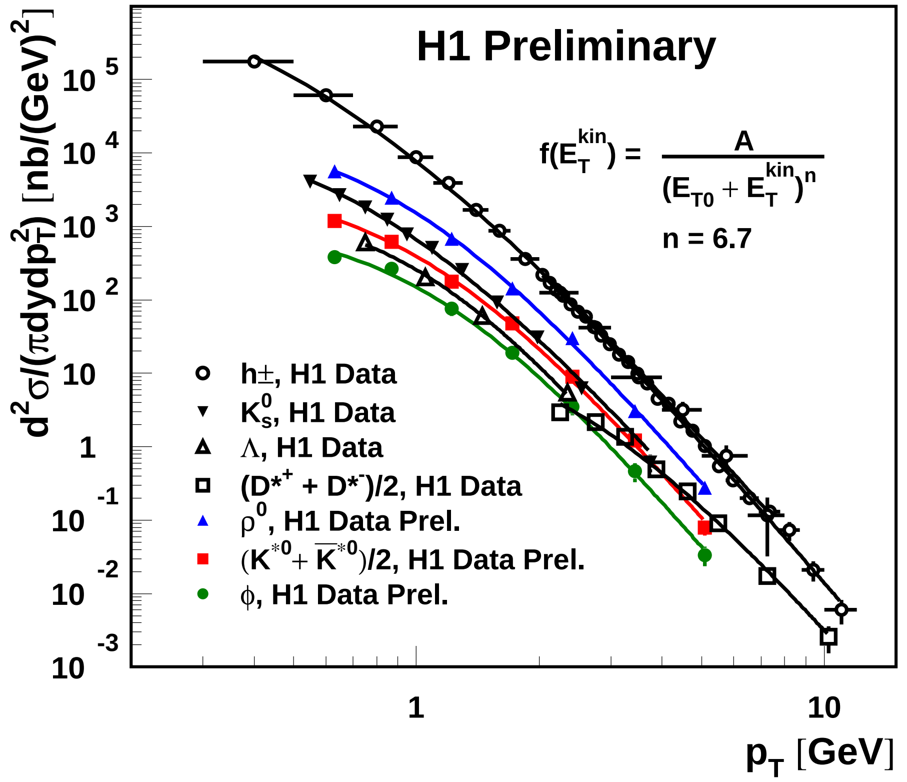

Figure 5: The differential non-diffractive cross-sections as a function of transverse momentum. The curves on the figure correspond to a damped power law fit using equation (1). Statistical and systematic errors are added in quadrature on these plots.